Prediction of Separated Transonic Wing Flows with Nonequilibrium Algebraic Turbulence Model

Ridha Abid* and Veer N. Vatsa†
NASA Langley Research Center, Hampton, Virginia 23665
Dennis A. Johnson‡
NASA Ames Research Center, Moffett Field, California 94035
and
Bruce W. Wedan‡
Vigyan, Inc., Hampton, Virginia 23665

A nonequilibrium algebraic turbulence model, which is based on the turbulence closure scheme of Johnson and King, is proposed to predict separated transonic wing flows. The influence of history effects are modeled by solving a partial differential equation for the maximum Reynolds shear stress, which is then used to scale the eddy viscosity of an algebraic model. The turbulence model is implemented in a three-dimensional, Reynolds-averaged Navier-Stokes code. Comparisons with experimental data are presented which show clearly that the nonequilibrium type of turbulence model is essential for accurate prediction of transonic separated flows.

Introduction

COMPUTATIONAL fluid dynamics is becoming an increasingly powerful tool in the aerodynamic design of aerospace vehicles as a result of improvements in numerical algorithms as well as in the processing speed and storage capacity of new generations of computers. However, many key pacing items limit the effectiveness of engineering computational fluid dynamics. Chief among these is turbulence modeling. Turbulent flows contain a very large range of length and time scales for adequate representation on current computers. Practical engineering calculations rely on phenomenological modeling of turbulence. This paper focuses on turbulence modeling in transonic flows.

Computations of two-dimensional transonic flows by solving the Reynolds-averaged Navier-Stokes equations revealed deficiencies in the turbulence modeling.[1] Equilibrium turbulence models, which assume that the turbulent shear stress depends only on local properties of the mean flow, give poor predictions for flows with strong shock-wave/boundary-layer interaction. The shock positions are predicted too far aft, and the pressure recovery is overpredicted. This is because the eddy viscosity does not account for the nonequilibrium between the turbulence and mean flow in the outer portions of the viscous layers. The use of a two-equation turbulence model, which does not use wall functions, increases computational costs and does not improve significantly the agreement of computed results with experimental data.[2] This is mainly due to the transport equation of the dissipation which is a purely empirical equation developed by analogy with that for turbulent kinetic energy. In principle, a good version of the latter type of model would have a greater range of applicability. In practice, the gap between performance and potential is still large.

Received Feb. 1, 1989; revision received Oct. 12, 1989.

*NRC Fellow; currently Research Scientist, Vigyan, Inc., Hampton, VA. Member AIAA.
†Senior Research Scientist. Member AIAA.
‡Research Scientist. Member AIAA.

Recently, Johnson and King[3] proposed a turbulence model for two-dimensional flows, which was based on a different philosophy from that used in developing the two-equation turbulence model. Instead of devising a universal model, they proposed a model for a specific class of flows which captures the most essential features of the flow. Their model accounts for history effects of the turbulence through an ordinary differential equation for the maximum of Reynolds shear stress. This maximum is then used to scale the eddy viscosity of an algebraic model. The Johnson-King model was found to perform well for transonic flows with strong viscous-inviscid interaction.[1]

In this paper, the nonequilibrium model of Johnson and King is extended to three-dimensional flows and is used to predict separated transonic wing flows. This model is implemented into a Reynolds-averaged Navier-Stokes code developed by Vatsa,[4] and Vatsa and Wedan,[5] which uses a Jameson type of time-stepping scheme to obtain steady-state solutions.

Governing Equations

High-Reynolds-number viscous flow over aerodynamic shapes is represented by the unsteady Navier-Stokes equations. These are specialized to a body-fitted coordinate system (ξ, η, ζ) where ξ, η, and ζ represent the streamwise, normal, and spanwise coordinates, respectively. For an isolated wing, the η-coordinate lines are nearly orthogonal to the wing surface. Since the dominant viscous effects for high-Reynolds-number flows arise from viscous diffusion normal to the body surface, a thin-layer assumption is employed here by retaining the viscous diffusion terms only in the η direction. For a stationary coordinate system, these equations can be written in the conservative law form as

$$\frac{\partial}{\partial t}(J^{-1}U)+\frac{\partial F}{\partial \xi}+\frac{\partial G}{\partial \eta}+\frac{\partial H}{\partial \zeta}=\frac{\partial G_v}{\partial \eta} \tag{1}$$

where

$$U=\begin{Bmatrix}\rho\\ \rho u\\ \rho v\\ \rho w\\ \rho E\end{Bmatrix} \tag{2}$$

$$F = J^{-1}\begin{Bmatrix} \rho\tilde{u} \\ \rho\tilde{u}u + \xi_x p \\ \rho\tilde{u}v + \xi_y p \\ \rho\tilde{u}w + \xi_z p \\ \rho\tilde{u}H \end{Bmatrix} \tag{3}$$

$$G = J^{-1}\begin{Bmatrix} \rho\tilde{v} \\ \rho\tilde{v}u + \eta_x p \\ \rho\tilde{v}v + \eta_y p \\ \rho\tilde{v}w + \eta_z p \\ \rho\tilde{v}H \end{Bmatrix} \tag{4}$$

$$H = J^{-1}\begin{Bmatrix} \rho\tilde{w} \\ \rho\tilde{w}u + \zeta_x p \\ \rho\tilde{w}v + \zeta_y p \\ \rho\tilde{w}w + \zeta_z p \\ \rho\tilde{w}H \end{Bmatrix} \tag{5}$$

$$G_v = \frac{\sqrt{\gamma}M_\infty}{Re_\infty}\frac{\mu\bar{\varepsilon}}{J}\begin{Bmatrix} 0 \\ \phi_1 u_\eta + \eta_x\phi_2 \\ \phi_1 v_\eta + \eta_y\phi_2 \\ \phi_1 w_\eta + \eta_z\phi_2 \\ \phi_1 a + \tilde{v}\phi_2 \end{Bmatrix} \tag{6}$$

where

$$\phi_1 = \eta_x^2 + \eta_y^2 + \eta_z^2 \tag{7}$$

$$\phi_2 = \tfrac{1}{3}(\eta_x u_\eta + \eta_y v_\eta + \eta_z w_\eta) \tag{8}$$

$$q^2 = u^2 + v^2 + w^2 \tag{9}$$

$$a = \left(\frac{q^2}{2}\right)_\eta + \left(\frac{\gamma}{\gamma - 1}\right)\frac{\tilde{\varepsilon}}{\sigma\bar{\varepsilon}}T_\eta \tag{10}$$

The contravariant velocity components used in Eqs. (3–6) are defined as

$$\tilde{u} = \xi_x u + \xi_y v + \xi_z w \tag{11}$$

$$\tilde{v} = \eta_x u + \eta_y v + \eta_z w \tag{12}$$

$$\tilde{w} = \zeta_x u + \zeta_y v + \zeta_z w \tag{13}$$

The transformation metrics are given by the following relations:

$$\begin{aligned} \xi_x &= J(y_\eta z_\zeta - y_\zeta z_\eta) & \zeta_y &= J(x_\eta z_\xi - x_\xi z_\eta) \\ \eta_x &= J(y_\zeta z_\xi - y_\xi z_\zeta) & \xi_z &= J(x_\eta y_\zeta - x_\zeta y_\eta) \\ \zeta_x &= J(y_\xi z_\eta - y_\eta z_\xi) & \eta_z &= J(x_\zeta y_\xi - x_\xi y_\zeta) \\ \xi_y &= J(x_\zeta z_\eta - x_\eta z_\zeta) & \zeta_z &= J(x_\xi y_\eta - x_\eta y_\xi) \\ \eta_y &= J(x_\xi z_\zeta - x_\zeta z_\xi) \end{aligned} \tag{14}$$

where J is the Jacobian of the transformation given by

$$J^{-1} = x_\xi(y_\eta z_\zeta - y_\zeta z_\eta) - y_\xi(x_\eta z_\zeta - x_\zeta z_\eta) + z_\xi(x_\eta y_\zeta - y_\eta x_\zeta) \tag{15}$$

In the preceding set of equations, distances have been nondimensionalized by a reference length L, taken to be the chord of the wing; density, pressure, and viscosity by their respective freestream values; and velocities by a reference velocity $u_{\text{ref}} = a_\infty/\sqrt{\gamma}$, where a_∞ is the freestream speed of sound; and enthalpy by u_{ref}^2. For an ideal gas, the total enthalpy is then given by the relation

$$\rho H = \left(\frac{\gamma}{\gamma - 1}\right)p + \rho\left(\frac{u^2 + v^2 + w^2}{2}\right) \tag{16}$$

In the governing equations presented here, the effects of turbulence are incorporated through the concepts of eddy viscosity and eddy conductivity. This is accomplished by replacing the molecular viscosity μ in the momentum equation by an effective viscosity μ_e, as follows:

$$\mu_e = \mu + \mu_t = \mu(1 + \mu_t/\mu) = \mu\bar{\varepsilon} \tag{17}$$

Similarly, the molecular conductivity k in the energy equation is replaced by the effective conductivity k_e, such that

$$\begin{aligned} k_e &= k + k_t = \frac{c_p}{\sigma}\mu + \frac{c_p}{\sigma_t}\mu_t \\ &= \frac{c_p}{\sigma}\mu\left(1 + \frac{\sigma}{\sigma_t}\frac{\mu_t}{\mu}\right) = \frac{c_p}{\sigma}\mu\bar{\varepsilon} \end{aligned} \tag{18}$$

Here σ and σ_t represent the laminar and turbulent Prandtl numbers, respectively. The details of the eddy-viscosity computational procedure are presented in a later section.

Computational Algorithm

In the present work, a semidiscrete finite-volume, pseudo-time-stepping scheme based on Jameson's Runge-Kutta scheme,[6-7] modified by Vatsa[4] and Vatsa and Wedan,[5] is used for obtaining steady-state solutions to the governing equations. A controlled amount of artificial dissipation is added to suppress odd-even points decoupling and the oscillations in the vicinity of the shock waves and stagnation points. Although the isotropic dissipation model originally proposed by Jameson and co-workers[6,7] is adequate for inviscid Euler equations, it is not very satisfactory for Navier-Stokes computations where highly stretched meshes are needed for accurate resolution of thin viscous layers. In order to obtain accurate numerical solutions on these highly stretched meshes, the nonisotropic model proposed by Martinelli[8] is employed here.

In order to increase the efficiency of the numerical scheme for obtaining steady-state solutions of the governing equations, a multigrid acceleration technique similar to the work of Refs. 8–10 is employed in the present code. A five-stage Runge-Kutta scheme with three evaluations of dissipation is employed in order to provide a larger stability zone and good damping properties for viscous flows (see e.g., Ref. 8). The multigrid acceleration is implemented via a full multigrid scheme employing V-cycles. The pertinent details related to the multigrid strategy employed for the three-dimensional Navier-Stokes equations are available in Ref. 11.

Turbulence Modeling

Algebraic turbulence models are not suitable for separated flows, because these models assume that locally the turbulent production and dissipation rates are in balance. To capture the correct physics of separated flow, nonequilibrium effects such as convection and diffusion of turbulence have to be taken into account. For this purpose, Johnson and King[3] proposed a new eddy viscosity model for two-dimensional separated flows. An ordinary differential equation is used to describe the development of the maximum turbulent shear stress, in conjunction with an assumed eddy viscosity distribution which has the maximum turbulent shear stress as its velocity scale. This model is extended to three-dimensional flows, as discussed here.

In order to effect smooth transition between the inner and outer eddy viscosity distribution, the turbulent eddy viscosity μ_t in the Johnson-King formulation, which is supposed to be isotropic, is assumed to have the functional form

$$\mu_t = \mu_{to}[1 - \exp(-\mu_{ti}/\mu_{to})] \tag{19}$$

The inner eddy viscosity μ_{ti} is given by

$$\mu_{ti} = \rho D^2 \kappa N \tau_m^{1/2} \tag{20}$$

where τ_m is the maximum Reynolds shear stress, N is the local normal distance from the wall, κ is the von Karman constant = 0.4, and D is the damping factor given by

$$D = 1 - \exp(-\rho_w N u_T / \mu_w A^+) \tag{21}$$

where, $A^+ = 17$ and u_T is given by

$$u_T = \max(\tau_m/\rho_m, \tau_w/\rho_w) \tag{22}$$

where, τ_w is the wall shear stress.

The Reynolds shear stress is assumed to be

$$\tau = \mu_t \Omega / \rho \tag{23}$$

where Ω is the magnitude of the vorticity.

The τ_m, which is invariant to the coordinate system, is obtained from the solution of a partial differential equation to be given below.

The outer eddy viscosity is determined by using the Baldwin-Lomax wake model,[12] instead of the Clauser wake model to avoid the necessity of finding the boundary-layer edge.

$$\mu_{to} = \bar{\sigma} \rho K C_c F_w \gamma_k \tag{24}$$

where K is the Clauser constant = 0.0168, $C_c = 1.6$, $F_w = N_{\max} F_{\max}$, and $F_{\max}$ is determined from the function

$$F(N) = N \Omega D \tag{25}$$

by locating the N value at which $F(N)$ is a maximum. In the separated region, the function F typically displays more than one peak. To obtain an unambiguous value of $F_{\max}$, we select the farthest peak away from the wall. Intermittency effects are accounted for by the Klebanoff intermittency factor γ_k:

$$\gamma_k = [1 + 5.5(N/\delta)^6]^{-1} \tag{26}$$

The modeling parameter $\bar{\sigma}$ provides the link between eddy viscosity distribution of Eq. (19) and the rate equation for the development of maximum Reynolds shear stress. By assuming that the structural parameter a_1, defined as the ratio of the Reynolds shear stress to the turbulent kinetic energy at the location of τ_m, is constant, a partial differential equation for the maximum Reynolds shear stress is derived from the turbulent kinetic energy.[13] In the Cartesian coordinate system, this equation is given by

$$\frac{\partial \tau_m}{\partial t} + U_m \frac{\partial \tau_m}{\partial x} + V_m \frac{\partial \tau_m}{\partial y} + W_m \frac{\partial \tau_m}{\partial z}$$

$$= \frac{a_1}{L_m} \tau_m [(\tau_{m,\mathrm{eq}})^{1/2} - \tau_m^{1/2}] - a_1 D_m \tag{27}$$

A time-dependent form of this equation is considered in the present paper so that the same algorithm, which is used for solving the main governing equations, can be used to solve it. Such a strategy is also useful for solving true time-dependent flows. In the preceding equation, the subscript m denotes a quantity evaluated at the location of the maximum Reynolds shear stress. The dissipation length scale L_m is specified as

$$L_m = \min(0.4\, N_m, 0.09\delta) \tag{28}$$

where δ is the boundary layer thickness, which is equal to $1.9 N_{\max}$. The quantity $\tau_{m,\mathrm{eq}}$ is assumed to be determined from the following equilibrium eddy viscosity distributions:

$$\mu_{t,\mathrm{eq}} = \mu_{to,\mathrm{eq}} \left| 1 - \exp(-\mu_{ti,\mathrm{eq}}/\mu_{to,\mathrm{eq}}) \right| \tag{29}$$

$$\mu_{ti,\mathrm{eq}} = \rho D^2 \kappa N \tau_{m,\mathrm{eq}}^{1/2} \tag{30}$$

$$\mu_{to,\mathrm{eq}} = \rho K C_c F_w \gamma_k \tag{31}$$

The turbulent diffusion term D_m was modeled by Johnson[14] as

$$D_m = \frac{C_D \tau_m^{3/2} |1 - \bar{\sigma}^{1/2}|}{a_1 [0.7\delta - N_m]} \tag{32}$$

Values of 0.25 and 0.5 were used for a_1 and C_D, respectively. The diffusion term D_m was found to have negligible effect in regions where the parameter $\bar{\sigma}$ was less than unity. In the present work, the diffusion term D_m was used only in the recovery regions.

Making the following change of variables

$$g = \tau_m^{-1/2} \tag{33}$$

$$g_{\mathrm{eq}} = (\tau_{m,\mathrm{eq}})^{-1/2} \tag{34}$$

a linear equation is obtained:

$$\frac{\partial g}{\partial t} + U_m \frac{\partial g}{\partial x} + V_m \frac{\partial g}{\partial y} + W_m \frac{\partial g}{\partial z} + \Gamma = 0 \tag{35}$$

where

$$\Gamma = \frac{a_1}{2L_m} \left[\left(\frac{g}{g_{\mathrm{eq}}} - 1 \right) - \frac{C_D L_m |1 - \bar{\sigma}^{1/2}|}{a_1 \delta (0.7 - N_m/\delta)} \right] \tag{36}$$

Using Gauss' theorem, Eq. (35) can be written:

$$\frac{\partial}{\partial t} \int_v g \, dv + U_m \int_{\delta v} g n_x \, ds + V_m \int_{\delta v} g n_y \, ds$$

$$+ W_m \int_{\delta v} g n_z \, ds + \int_v \Gamma \, dv = 0 \tag{37}$$

where v is the volume of a cell with a boundary δv; and n_x, n_y, n_z are the components of the outward normal vector to the surface δv.

A cell-centered finite-volume discretization of Eq. (35) is applied to each cell of the computational domain. A system of ordinary differential equations in time is obtained which is solved by the explicit five-stage Runge-Kutta time-stepping scheme discussed earlier in the paper. The convergence is accelerated to steady state by local time stepping.

Solutions based on this model are obtained as follows. First, a steady-state solution is obtained by using the equilibrium model (the parameter $\bar{\sigma}$ was set up equal to unity). Then the Johnson-King model is activated after 35 cycles. At each time advance, two values of the maximum shear stress are determined; one based on the maximum value of $\mu_t \Omega$ from Eq. (23) and the other τ_m based on the integration of Eq. (35). These two are then used to update $\bar{\sigma}$ at the next time level according to the following relation:

$$\bar{\sigma}^{t + \mathrm{d}t} = \bar{\sigma}^t \frac{\rho_{\max} \tau_m}{(\mu \Omega)_{\max}} \tag{38}$$

Results and Discussion

The test case of turbulent flow over the ONERA M6 wing at Mach number (M_∞) of 0.84, angle of attack (α) of 6.06 and a Reynolds number (R_e) of 11.7×10^6 based on the mean aerodynamic chord and freestream conditions is used in the present study. This test case has also been investigated in previous studies[4,15] due to the availability of detailed experimental surface pressure data.[16] A c-o type of grid, shown schematically in Fig. 1, is employed here. In this paper, the effect of grid refinement on the computational results will be presented in order to eliminate the concerns of inaccuracies

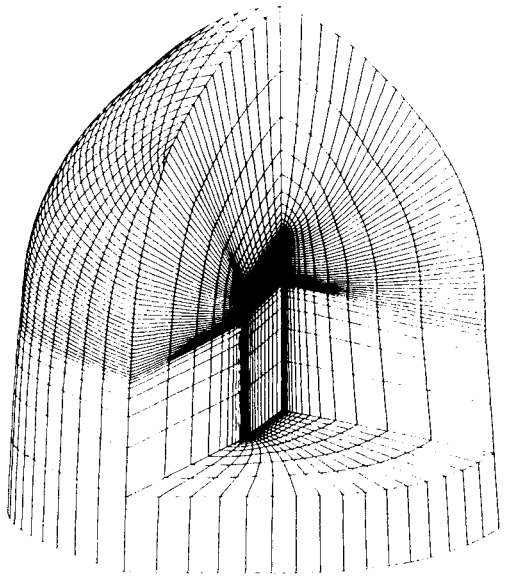

Fig. 1 Schematic view of computational grid for ONERA M6 wing.

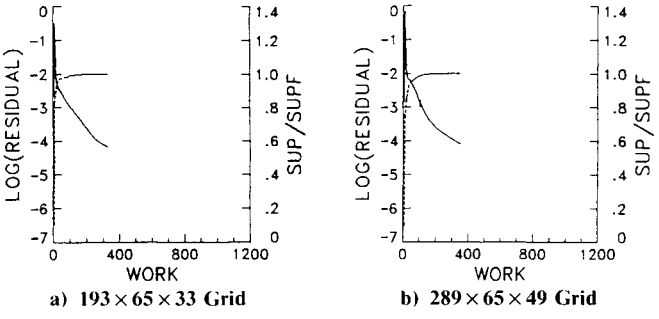

Fig. 2 Effect of grid refinement on convergence history for ONERA M6 wing (Baldwin-Lomax model: $M_\infty = 0.84$, $\alpha = 6.06$ deg).

due to grid resolution. In addition, results obtained with Baldwin-Lomax and Johnson-King turbulence models will be shown in order to assess the effect of nonequilibrium terms in the turbulence model.

Effect of Grid Refinement

During this phase of the investigation, the standard Baldwin-Lomax model is employed. The first set of calculations were performed on a medium-resolution grid containing 193 × 65 × 33 points in the streamwise, normal, and spanwise directions, respectively. The distance to the first grid-point away from the wall is 10^{-5} local chord lengths, resulting in y^+ values between 3 and 5 for most part of the wing. Such a mesh, with a total of 413,985 nodes, would be considered a fine mesh for most existing codes due to the large computer resources required for obtaining converged solutions. However, the availability of an efficient multigrid code[11] makes it feasible to compute such flows on much finer meshes in order to study the effect of grid refinement.

The convergence history for this case, in terms of residual of the continuity equation and number of supersonic points (normalized by its final value), is shown as a function of work units in Fig. 2a. A work unit here represents the equivalent of a computational effort for one fine-mesh iteration, and is regarded as a good representative of true computational work in the multigrid context. It is observed from this figure that the residual dropped by four orders in approximately 300 work units, which took approximately 1.6 h on a Cray 2 computer. It should be pointed out that the supersonic zone and lift for this case converged in less than 200 work units. The computations were also performed on a finer grid consisting of 289 × 65 × 49 mesh points, for a total of 920,465 node points. This mesh was obtained by increasing the mesh resolution in the streamwise and spanwise directions by 50%. The normal mesh resolution was kept the same, since the effect of increasing normal mesh resolution on pressure distributions was found to be minimal for this case. The resulting convergence history on the fine mesh (289 × 65 × 49) is shown in Fig. 2b. Again four orders of reduction in the residual are obtained in about 300 work units, which required approximately 3 h of CPU time on a Cray 2 computer. It is noticed that there is only a slight deterioration in the convergence rate due to grid refinement.

The computed pressure distributions are compared with the experimental data at four spanwise locations in Fig. 3. It is observed that the effect of refining the grid on the computed pressure distributions is only minor and localized. The grid-refinement results mainly in sharper shocks and suction peaks. The pressure correlation with the data is considered poor, particularly in the outboard part of the wing. Similar results using Baldwin-Lomax model have been reported previously in the literature for this case.[4,15] Based on the present grid-refinement study, it is obvious that the disagreement with the data is not due to the coarseness of the mesh. It is believed that the use of an equilibrium type of turbulence model, namely the Baldwin-Lomax model, results in the underprediction of the reverse flow region and hence the predicted shocks are found to lie downstream of their experimental counterparts. This, in turn, results in overprediction of the pressure behind the shock and a poor overall agreement with the data.

Effect of Turbulence Model

It was observed in the previous section that the standard Baldwin-Lomax turbulence model is inadequate for accurate prediction of the the transonic flow for the test case selected here. In order to quantitatively assess the nonequilibrium effects of the turbulence model, computations were repeated for the fine mesh (289 × 65 × 49) using the Johnson-King turbulence model described earlier in the paper. The conver-

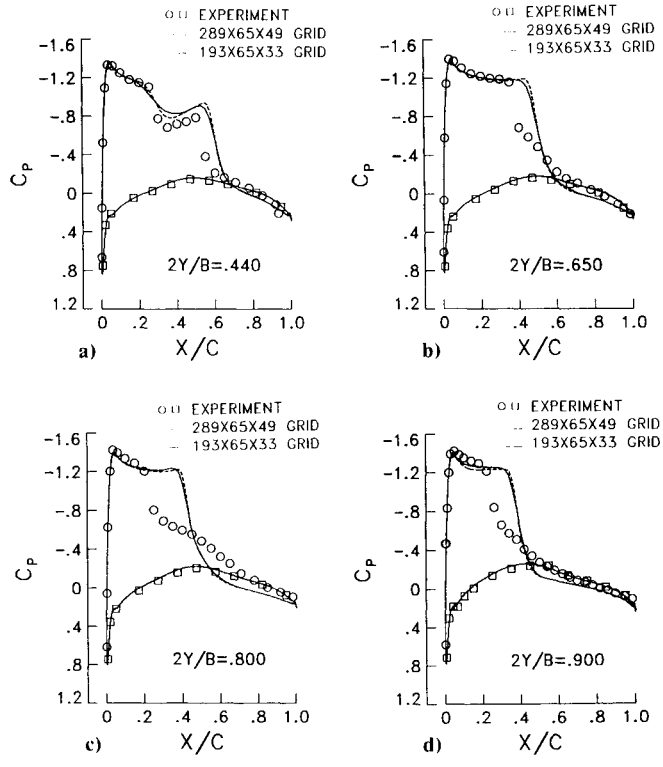

Fig. 3 Effect of grid refinement on pressure distribution for ONERA M6 wing (Baldwin-Lomax model: $M_\infty = 0.84$, $\alpha = 6.06$ deg).

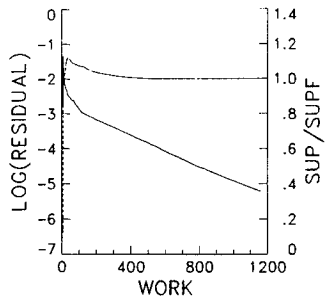

Fig. 4 Convergence history for ONERA M6 wing for 289 × 65 × 49 grid (Johnson-King model: $M_\infty = 0.84$, $\alpha = 6.06$ deg).

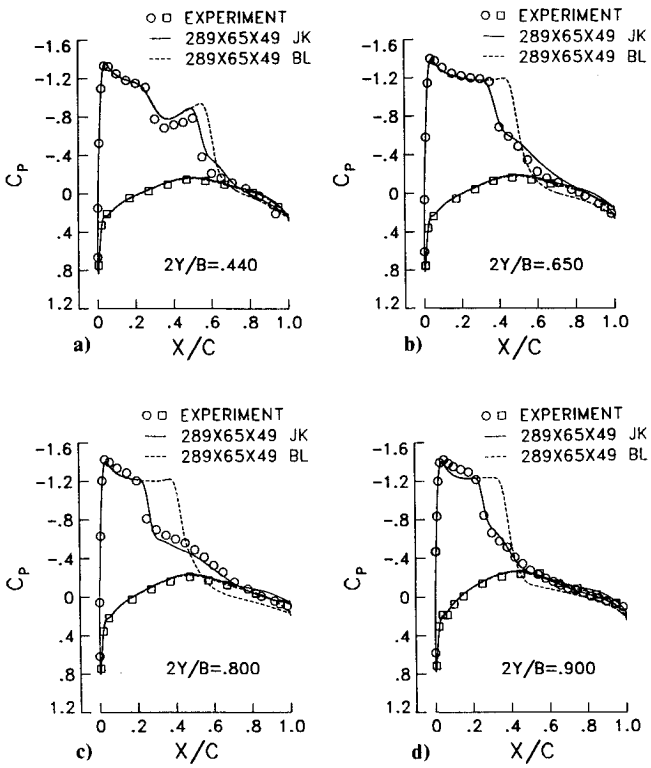

Fig. 5 Effect of turbulence model on pressure contours for upper surface of ONERA M6 wing (289 × 65 × 49 grid, $M_\infty = 0.84$, $\alpha = 6.06$ deg).

gence history for this case is shown in Fig. 4. The solutions in the full multigrid sequence were initiated with freestream conditions on the 145 × 33 × 25 mesh, where the equilibrium turbulence model was employed. The full nonequilibrium model ($\bar{\sigma}$ not equal to unity) was turned on after 35 cycles on the 289 × 65 × 49 mesh. It is noted from this figure that the convergence for this case is slower compared to the case where the Baldwin-Lomax model was employed. It took approximately 550 work units to obtain a reduction of four orders in the residual, and the convergence of the supersonic zone and lift showed similar deterioration. However, one must realize that the degree of nonlinearity in the physical problem has increased significantly due to the nonequilibrium model of Johnson-King, which is more dynamic in nature. This increased nonlinearity due to the coupling of $\bar{\sigma}$ and τ_m [see Eqs. (27) and (32)] results in the slowdown of convergence observed here. Similar observations in slowdown convergence for more sophisticated and nonequilibrium type of turbulence models have been reported by other researchers also.[1-2]

The computed pressure distributions using the Johnson-King model are compared with the experimental data in Fig. 5. The results obtained using the Baldwin-Lomax turbulence model are also plotted in this figure for comparison. It is clear from this figure that the nonequilibrium effects for this case are very significant and the solutions obtained with the Johnson-King model are in excellent agreement with the data. The predicted shock locations are much closer to the data and the computed pressure distributions in the postshock region reproduce the data very accurately, including the pressure plateau region which was not observed in previous computations that employed the Baldwin-Lomax model.

The pressure contours for the upper surface of the wing based on present calculations are compared in Fig. 6. From this figure, it is observed that the shock position, particularly in the outboard part of the wing, is predicted much further upstream and is much stronger for the Johnson-King model than for the Baldwin-Lomax model. This is because the Johnson-King model produces lower values of eddy viscosity

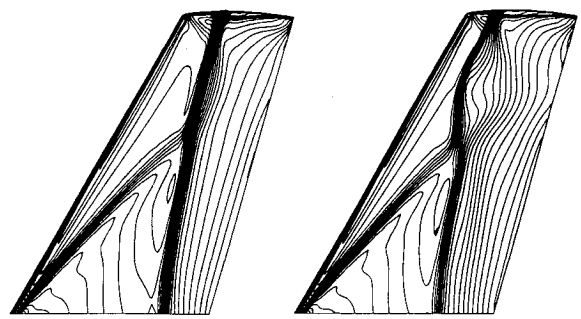

a) 193 × 65 × 33 Grid b) 289 × 65 × 49 Grid

Fig. 6 Effect of turbulence model on pressure distributions for ONERA M6 wing (289 × 65 × 49 grid, $M_\infty = 0.84$, $\alpha = 6.06$ deg).

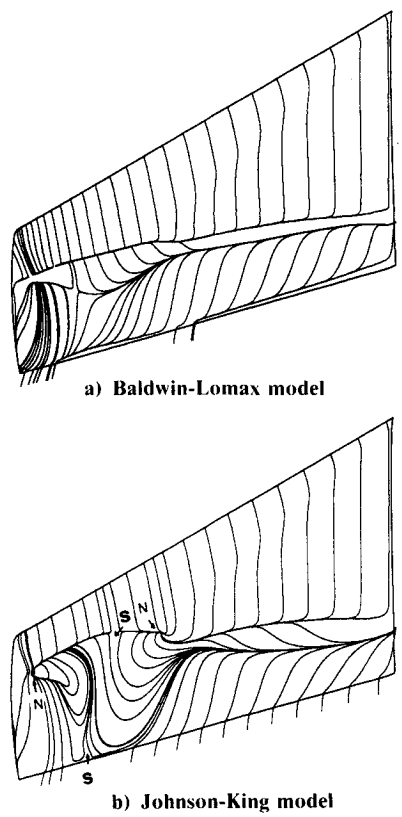

a) Baldwin-Lomax model

b) Johnson-King model

Fig. 7 Effect of turbulence model on streamline pattern for upper surface of ONERA M6 wing (289 × 65 × 49 grid, $M_\infty = 0.84$, $\alpha = 6.06$ deg; N—node point S—saddle point).

in adverse pressure gradient regions. This results in a thicker boundary layer and upstream movement of the shock, which in turn produces a larger reverse flow region seen in Fig. 7, where the surface streamline patterns for the upper surface are shown for both the Baldwin-Lomax and the Johnson-King models. It is readily observed that the extent of the reverse flow zone predicted with the Johnson-King model is much larger compared to the Baldwin-Lomax results, particularly in the outboard part of the wing. The Baldwin-Lomax results display a small streamwise reverse flow zone over most of the wing, with a very simple topological structure. The streamlines emanate along an attachment line and terminate along a separation line. The Johnson-King results, by contrast, display a much more complex topology in the streamline pattern, particularly on the outboard sections. These solutions indicate the presence of two regions of counter-rotating flows, one emanating from and the other terminating in a node (see Ref. 17 for these definitions). Two saddle points are also seen in this figure. Although, there is no surface flow visualization data available for the present test case, the overall flow pattern (shown in Fig. 7), sometimes referred to as a mushroom structure, has also been observed experimentally under transonic conditions for flow over lifting wings.[18] Coupled with the excellent correlation that is obtained with the pressure data, it is believed that these results represent a significant step towards developing computational capability for predicting three-dimensional transonic separated flows.

Concluding Remarks and Future Directions

The nonequilibrium algebraic model of Johnson and King has been extended to three-dimensional flows. The proposed model has been implemented in a three-dimensional Navier-Stokes code. Solutions have been presented here for high-Reynolds-number transonic flow over a transport wing. The results presented here clearly indicate that nonequilibrium effects have to be incorporated in the turbulence models for accurate prediction of transonic flows in the presence of reverse flow regions. Navier-Stokes solutions with the Johnson-King model compare very well with pressure data and the resulting streamlines on the wing surface reproduce the mushroom structure observed experimentally in other transonic separated flows.

However, the present turbulence model cannot be considered entirely satisfactory for flows with strong crossflow velocities. The Johnson-King model, like the two-equation models, are not able to reproduce the anisotropy of eddy viscosity. In fact, three-dimensional boundary-layer experiments showed that the eddy viscosity is not isotropic. To capture this effect of the three-dimensionality, Abid[19] proposed an anisotropic eddy viscosity model for three-dimensional boundary layers which is based on the turbulence closure of Johnson and King. A further refinement of the nonisotropic model is needed before implementing it in a three-dimensional Navier-Stokes code.

Acknowledgment

The authors wish to express their gratitude to Rolf Radespiel for his help in developing the time-dependent solution procedure for the partial differential equation associated with the Johnson-King model.

References

[1]Holst, T. L., "Viscous Transonic Airfoil Workshop Compendium of Results," AIAA Paper 87-1460, Jan. 1987.

[2]Coakley, T. J., "Numerical Simulation of Viscous Transonic Airfoils Flows," AIAA Paper 87-0416, Jan. 1987.

[3]Johnson, D. A., and King. L. S., "A Mathematically Simple Turbulence Closure Model for Attached and Separated Turbulent Boundary Layers," *AIAA Journal*, Vol. 23, Nov. 1985, pp. 1684–1692.

[4]Vatsa, V. N., "Accurate Numerical Solutions for Transonic Flow Over Finite Wings," *Journal of Aircraft*, Vol. 24, June 1987, pp. 377–385.

[5]Vatsa, V. N., and Wedan, B. W., "Navier-Stokes Solutions for Transonic Flow Over a Wing Mounted in a Tunnel," AIAA Paper 88-0102, Jan. 1988.

[6]Jameson, A., Schmidt, W., and Turkel, E., "Numerical Solutions of the Euler Equations by Finite-Volume Methods Using Runge-Kutta Time-Stepping Schemes," AIAA Paper 81-1259, June 1981.

[7]Jameson, A., and Baker, T. J., "Solution of the Euler Equations for Complex Configurations," AIAA Paper 83-1929, July 1983.

[8]Martinelli, L., "Validation of a Multigrid Method for the Reynolds-Averaged Equations," AIAA Paper 88-0414, Jan. 1988.

[9]Jameson, A., "Transonic Flow Calculations," Dept. of Mechanical and Aerospace Engineering, Princeton Univ., Princeton, NJ, MAE Rept. 1651, 1987.

[10]Swanson, R. C., and Turkel, E., "Artificial Dissipation and Central-Difference Scheme for the Euler and Navier-Stokes Equations," AIAA Paper 87-1107, June 1987.

[11]Vatsa, V. N., and Wedan, B. W., "Development of an Efficient Multigrid Code for Three-Dimensional Navier-Stokes Equations," AIAA Paper 89-1791, June 1989.

[12]Baldwin, B. S., and Lomax, H., "Thin-Layer Approximation and Algebraic Model for Separated Turbulent Flows," AIAA Paper 78-257, Jan. 1978.

[13]Abid, R., "Extension of the Johnson-King Turbulence Model to the 3-D Flows," AIAA Paper 88-0223, Jan. 1988.

[14]Johnson, D. A., "Predictions of Transonic Separated Flow with an Eddy Viscosity/Reynolds Shear Stress Closure Model," AIAA Paper 85-1638, July 1985.

[15]Jayaram, M., and Jameson, A., "Multigrid Solution of the Navier-Stokes Equations for Flow Over Wings," AIAA Paper 88-0705, Jan. 1988.

[16]Schmitt, V., and Charpin, F., "Pressure Distributions on the ONERA M6 Wing at Transonic Mach Numbers," AGARD-AR-138, Chap. B-1, May 1979.

[17]Tobak, M., and Peake, D. J., "Topology of Two-Dimensional and Three-Dimensional Separated Flows," AIAA Paper 79-1480, July 1979.

[18]Lockman, W. K., and Seegmiller, H. L., "An Experimental Investigation of the Subcritical and Supercritical Flow About a Swept Semispan Wing," NASA TM-84376, June 1983.

[19]Abid, R., "An Anisotropic Eddy Viscosity for 3-D Separated Boundary-Layer Flows," Society of Automotive Engineers, Warrendale, PA, Paper 88-1544, Oct. 1988.